Physical Modelling in Geotechnics

Cantilever steel tubular pile wall embedded in stiff ground subjected to sequential dynamic and static loadings

S.M. Shafi & J. Takemura
Department of Civil & Environmental Engineering, Tokyo Institute of Technology, Japan

V. Kunasegaram
Department of Civil Engineering, South Eastern University of Sri Lanka, Sri Lanka

ABSTRACT: A key concern in applying a Cantilever-type Steel Tubular Pile (CSTP) wall is the stability under ultimate loading conditions, such as strong dynamic excitations and saturated backfill conditions. In this study, three centrifuge model tests were conducted to study the mechanical behavior of the CSTP walls subjected to such extreme lateral and moment loads at 50g centrifugal acceleration. CSTP walls with 12m retained height and 2.5 m,3 m embedment depths in soft rock were tested under different static and dynamic loading sequences. Based on the findings, the elastic resilience of the wall formed by the confinement of soft rock was a critical factor that influences the earth pressure, the dynamic and residual displacements of the wall. Furthermore, a 0.5m increase in embedment depth enhanced the wall's stability under both static and intense dynamic excitations.

Keywords: embedded cantilever wall, steel tubular pile, soft rock, earthquake, water pressure

1 INTRODUCTION

A cantilever retaining wall has several advantages over the conventional retaining wall because of its less redundancy on the additional support. This advantage makes it suitable to apply in the urban areas of Japan (see Fig. 1 (a)). The application of Steel Tubular Piles (STP) as retaining structure has increased in the past decades due to technological advancements like rotary cutting technique (Matsuzawa et al., 2021). In soft soil, the application of Cantilever Type Steel Tubular Piles (CSTP) walls has limitations in the wall height due to relatively large deflection. However, in the stiff ground like soft rock, large retain height is possible if used large diameter STP (Miyanohara et al., 2018). As shown in Fig. 1 (b), a CSTP wall is not only subjected to the lateral pressure from retained soil but also some extreme external loading like an earthquake, an increase in water level in the backfill side, or the combination of both. Two possible combinations of loading could be expected during the service period of the CSTP wall, like an earthquake(dynamic)-Water level rise in the back (static) or vice versa. One of the ways to withstand such extreme lading could be increasing the penetration depth. However, based on the Association of Steel pipe Pile (ASP, 2009) guideline which is based on famous Chang's, (1934) method, the allowable penetration depth will be over-conservative if used for stiff ground (Shafi et al., 2021). This research aims to study the mechanical behavior of the CSTP wall subjected to such extreme loading conditions with penetration depth less than the guideline proposed by ASP, (2009).

Table.1 Test conditions and material properties

Test code	Embedment soft and backfill sand	Rock socket depth: d_r ( )$, [$\beta d_r$] {FS at h_w=0m} <FS at h_w=8m >	Wall/Pile Properties Φ, t, EI, M_y ( )$
Case 1 **C1**	Toyoura sand: (Dr=85%): γ_d=15.8kN/m^3 ϕ'=42° Soft rock: γ_t=20.1kN/m^3 q_u=1.4MPa E_s=660MPa	3.0m (60 mm) **[1.2] {2.3} <1.6>**	Φ=2m (40 mm) t= 25mm (0.5 mm) Spacing: 2.15m (43 mm) EI= 6.8 GNm^2/m (5.4x10^{-5}GNm^2/m) M_y= 9.0 MNm/m (3.6x10^{-3} MNm/m)
Case 3 **C3**		2.5m (50 mm) **[1.0] {1.9} <1.3>**	
Case 6 **C6**		2.5m (50 mm) **[1.0] {1.9} <1.3>**	

$:(model scale); βd_r: normalized depth of model CSTP wall;

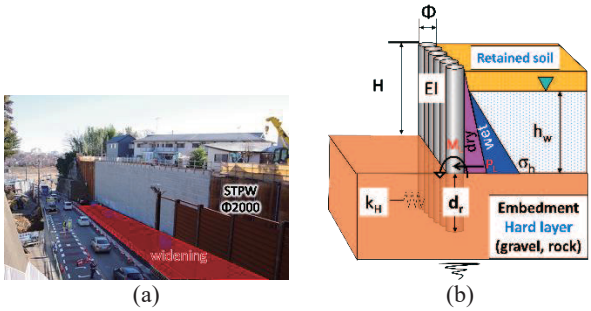

(a) (b)

Fig. 1. (a) Real application of CSTP wall in Japan (Kitamura and Kitamura, (2019)) (b) Typical CSTP wall.

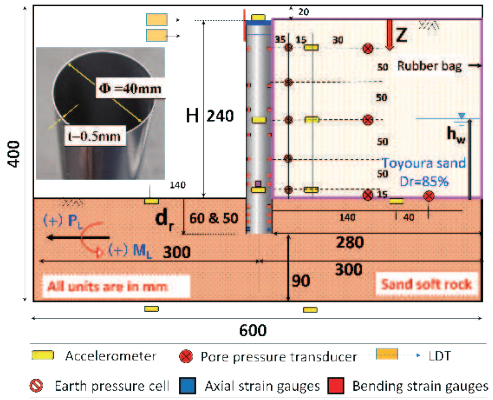

Fig. 2. 2D view of the model.

2 MODEL DESCRIPTIONS AND TEST CONDITIONS

The plan view of the model is illustrated in Fig. 2. The model was made under 50g centrifugal acceleration. The model was designed to represent a permanent or temporary CSTP wall retaining H=12m soil with pile diameter (Φ) and thickness (t) of 2m & 25mm in prototype scale.

A rigid frame container with inner dimensions 600mm X 400mm X 250mm was used to prepare the model. The model structure was consisted of five steel tubular piles (SUS304) connected at the head and spanned the width of the container to maintain a plane strain condition. A rubber bag was used to contain the backfill soil and to create a water-tight environment in the back. The backfilling was done by air pluviation technique using Toyoura sand. More details about the preparation of the model and sensors can be found in Shafi et al., (2021). An artificially prepared soft rock with unconfined compressive strength (q_u) of 1.4MPa (on the 14th day of curing) was used as supporting ground. This soft rock was prepared by sand-clay-cement, mixed with the appropriate amount of water. More detail about the preparation of the artificial soft rock can be found in Kunasegaram & Takemura, (2021).

The details of the test conditions are given in Table 1. All the properties were identical in all the tests, except for the socketing depth (d_r). Case 1 had d_r =3.0m, and cases 3 and 6 had d_r=2.5m; smaller than the ASP (2009) recommendation (d_r=7.5m) calculated based on this model conditions. The stability of the model CSTP wall was checked using the pressure distribution given by Padfield and Mair, (1984). In this paper, factor of safety is defined by ($d_r/d_{r(critical)}$), calculated assuming ϕ=0° below dredge level and pivotal point located at the toe of the wall. The calculated FS for different water level (h_w) is shown in Table 1.

All the cases consisted of dynamic and static events as illustrated in Fig. 3. A sinusoidal wave of predominant frequency 1Hz was applied as dynamic loading, as shown in Fig. 3 (d). Water was supplied in the back

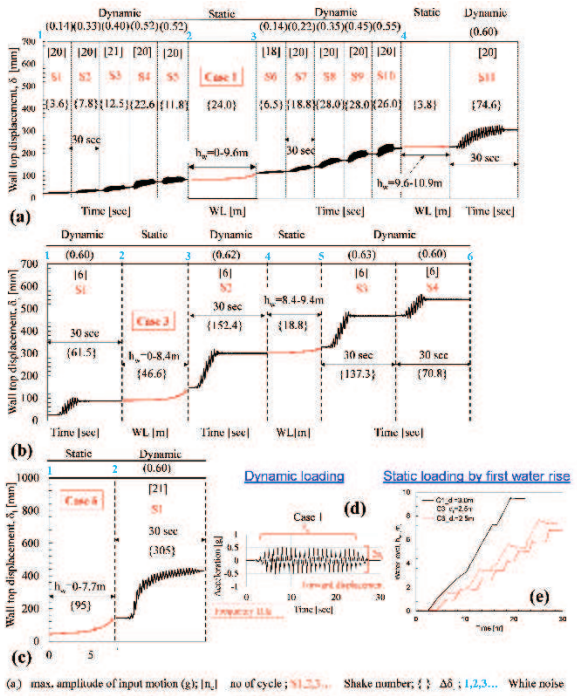

Fig. 3. Loading sequence and histories (a) case 1:dr=3.0m (b) case 3:dr=2.5m (c) case 6:dr=2.5m (d) typical dynamic loading (e) Typical static loading.

following the sequence (first water rises), as shown in Fig. 3 (e). Case 1 and 3 had the same initial loading event, dynamic followed by static loading by water rise. However, in case 6, static loading was applied first than dynamic loading. Based on the loading sequences, the initial condition of static loading in case 6 can be characterized as without pre-shaking and cases 1 and 3 as with pre-shaking. The outcome of applied loading is shown as measured wall top displacement by LDTs in Fig. 3 (a), (b), and (c) for cases 1, 3, and 6, respectively.

3 RESULTS AND DISCUSSIONS

Unless stated otherwise, all the discussions will be based on the prototype scale.

Fig. 4 shows the typical time history of measured wall top displacement (δ_t) and lateral pressure (σ_h) at different depths during case 1 shake 4. Here, the solid bold line represents residual (static component) displacement/lateral pressure accumulation during shaking. The observed dynamic component of lateral pressure at shallow depth is higher than the deepest, as commonly expected in the field during an earthquake. Furthermore, the observed residual earth pressure increased with residual wall top displacement. This behavior can be interpreted as, although the wall is moving forward, but the lateral pressure is increasing instead of decreasing. This phenomenon occurred due to the large confinement from rock and the elastic resilience of the wall and is termed as the "resilience effect" in this paper.

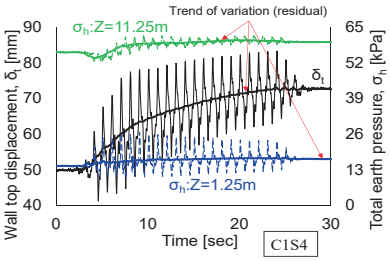

Fig. 4. Time history of measured displacement and earth pressure.

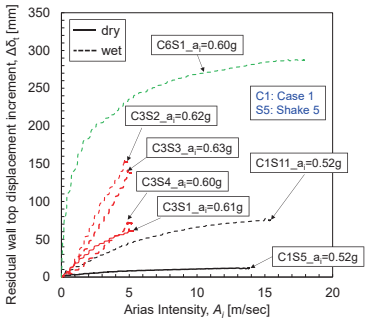

Fig. 5. Accumulation of residual wall top displacement during dynamic loading.

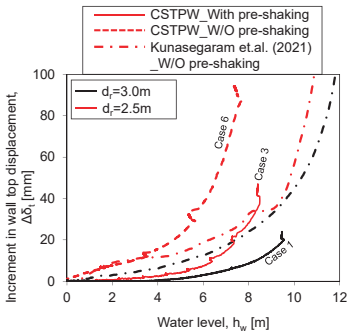

Fig. 6. Increment in wall top displacement by static loading.

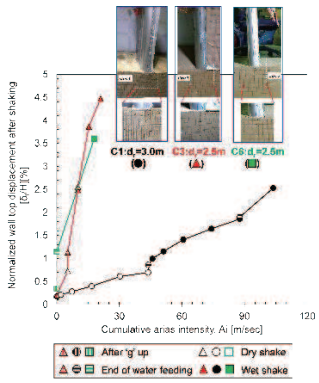

Fig. 7. Summary of wall top displacement.

3.1 Effect of rock socketing depth

From Fig. 3 (a), (b), and (c), accumulation of residual displacement by loadings is observed in all the cases. To understand the effect of dynamic loading on wall top displacement, the increment in residual wall top displacement is plotted against the Arias intensity (A_i) defined by equation 1 in Fig. 5. With the increase in the number of loadings, the rock confinement deteriorates, which can be evident from the large displacement by C1S11 than C1S5. However, the observed displacement for C3S4 is smaller than C3S3. Because of the almost similar magnitude of the earthquake in the previous shaking (C3S3), the developed resilience prevented the wall from accumulating large displacement during C3S4. Overall, the residual displacement accumulated by d_r=3.0m is smaller than d_r=2.5m during dynamic loading.

The increment in wall top displacement during static loading by water rise in the back is illustrated in Fig. 6. Also, the wall top displacement observed by Kunasegaram & Takemura, (2021) for their simplified (2D plate) wall model with the same retain height is shown in this figure.

The increment in wall top displacement during static loading by water rise in the back is illustrated in Fig. 6. Also, the wall top displacement observed by Kunasegaram & Takemura, (2021) for their simplified (2D plate) wall model with the same retain height is shown in this figure.

That simplified wall model was equivalent to the steel tubular pile wall model. However, only static loading by water rise was applied to the wall without shaking. The measured wall top displacement for d_r=3.0m < d_r=2.5m under identical water level (h_w) for CSTP wall. Similar observation was made for 2D plate wall model. Case 6 of CSTP wall and 2D plate wall model with d_r=2.5m had similar loading history (without pre-shaking). However, the observed wall top displacement by 2D plate wall model is smaller than the CSTP wall model at large water level (h_w>0.3H) as shown in Fig. 6.

Fig. 7 summarized the residual displacement observed after each loading for case 1, 3 and 6. The displacements are normalized by wall height and plotted against the cumulative Arias intensity. Also, the wall and ground condition after the tests are shown in this figure. The observed wall top displacement for d_r=2.5m (C3) is about 1.75 times d_r=3.0m (C1). Therefore, the mobilized resistance of the wall against extreme loading could be improved by increasing the rock socketing depth by 0.5m.

The observed wall top displacement by C6S1 in Fig. 5 is about 2.5%H. However, from concave shape variation between A_i-δ_t confirms that the rock can still resist the loading. Overall, the observed wall top displacement in Fig. 7 by d_r=2.5m is over 3.5%H, yet no catastrophic failure was noticed. This observation confirms that the stability against catastrophic failure of the CSTP wall could be well maintained even at rock socketing depth smaller than the recommended rock socketing depth by ASP (2009).

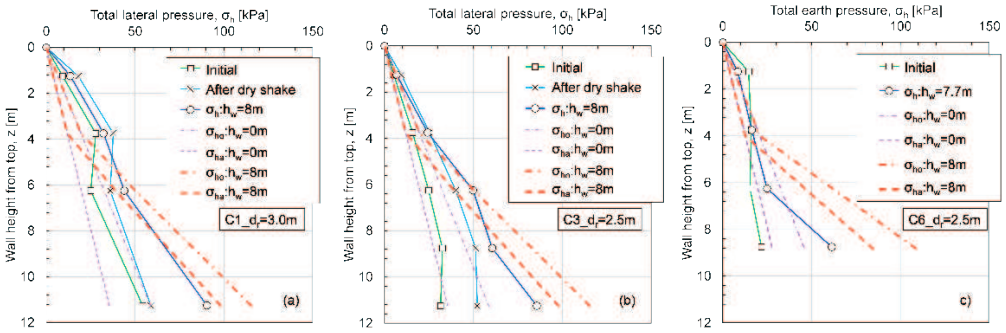

Fig. 8. Lateral pressure distribution (a) case 1:dr=3.0m (b) case 3:dr=2.5m (c) case 6:dr=2.5m.

3.2 Effect of pre-shaking

The initial condition of first static loading in cases 1, 3, and 6 is mentioned in article 2. Similarly, the initial condition 2D plate wall model can be characterized as a wall without pre-shaking.

In Fig. 5, for identical arias intensity, the observed displacement by C6S1 is higher than C3S2. Here, C6S1 previously had only static loading; however, C3S2 previously had both static and dynamic loading. In Fig. 6, the observed wall top displacement for case 6 is higher than case 3. Similarly, observed wall top displacement by 2D plate wall model with d_r=2.5m showed large displacement compared to case 3 (d_r=2.5). Therefore, it can be said that the loading history influence the wall displacement behavior ($\delta_{t\,(W/O\ pre\text{-}shaking)} > \delta_{t\,(With\ pre\text{-}shaking)}$).

The lateral pressure (σ_h) distribution with depth is shown in Fig. 8, along with the reference at-rest (σ_{ho}) and active pressure (σ_{ha}). Here, "Initial" refers to the earth pressure after the g-up, and "After dry shake" refers to earth pressure after the dry shaking events. The initial (σ_h) for d_r=3.0m is higher than the d_r=2.5m (see Fig. 8 (a) and (b)). This behavior confirms the effect of rock socketing depth on (σ_h). For cases 3 and 6, the initial (σ_h) is close to (σ_{ha}) (see Fig. 8 (b) and (c)).

In Fig. 8 (a) and (b), the (σ_h) increased after the dynamic event, although the displacement increased (see Fig. 4 (a) and (b)). This behavior confirms the "resilience effect" as mentioned previously. Therefore, the initial condition (σ_h) before the static loading in case 3 becomes higher than case 6 initial condition (σ_h). This increase in (σ_h) prevented the wall from immediately initiating the active condition, causing a small increase in wall top displacement at shallow water level ($h_w \approx 0.3H$) (see Fig. 6). The (σ_h) distribution at h_w about 8m for case 6 is much smaller than case 3. This behavior justifies the large displacement observed by C6S1 than C3S2 shown in Fig. 5.

4 CONCLUSIONS

Based on the test condition provided in this paper, it can be concluded that:

The wall resistance against static and dynamic loading can be increased significantly by increasing 0.5m rock socketing depth. Also, the stability of the CSTP wall could be ensured against the catastrophic failure by extreme loading conditions mentioned in this paper with rock socketing depth one-third smaller than the ASP (2009) guideline.

The resilience effect developed by the dynamic loading showed a positive effect during static loading by water rise, especially at shallow water levels.

Although the difference in several factors (like flexural rigidity, geometry of the wall) could influence the wall top displacement behavior. However, the wall top displacement observed for the 2D plate model by Kunasegaram & Takemura, (2021) is smaller than the actual CSTP wall.

ACKNOWLEDGEMENTS

The authors gratefully acknowledge the individual advice and guidance provided by the members and advisers of the IPA TC1.

REFERENCES

Association of Steel Pile (ASP). 2009. *Design manual of self-standing steel sheet pile wall*. (In Japanese)

Chang Y.L. 1937. Lateral pile loading tests. *Transaction of ASCE* 102: 273–276.

Kitamura, M. and Kitamura, S. 2019. Cantilevered Road Retaining Wall Constructed of 2,000mm Diameter Steel Tubular Piles Installed by the Gyro Press Method with GRB system. *Press-in Piling Case History, IPA,* Vol. 1: 41-48.

Kunasegaram V. and Takemura J. 2021. Deflection and failure of high stiffness cantilever retaining wall embedded in soft rock. *Intn J. Physical Modelling in Geotechnics* 21(3): 114–134,

Matsuzawa K., Hayashi T. Shirasaki K. 2021. Case study Ebitori river. *Proceedings of the Second International Conference on Press-in Engineering, June 2021.* Kochi, Japan.

Miyanohara T., Kurosawa T., Harata N. et al. 2018. Overview of the self-standing and high stiffness tubular pile walls in Japan. *In Proceedings of the 1st International Conference on Press-in Engineering, September 2018.* Kochi, Japan.

Padfield, C.J. and Mair, R.J., 1984. *Design of retaining walls embedded in stiff clay*. CIRIA report 104, CIRIA, London.

Shafi S.M., Takemura J., Kunasegaram V., Ishihama Y. Toda K., Ishihara Y. 2021. Dynamic behavior of cantilever tubular steel pile retaining wall socketed in soft rock. *Proceedings of the Second International Conference on Press-in Engineering, June 2021.* Kochi, Japan.